Investigation on Influence Parameter of Aircraft-Missile Separation by Considering Aeroelasticity

Yishan ZHANG[1,2], Hao ZHAN[1,2], Baigang MI[1,2], Mingxuan ZHANG[1,2]

[1] School of Aeronautics of Northwestern Polytechnical University, Xi'an 710072, China
[2] National Key Laboratory of Aircraft Configuration Design, Xi'an, 710072, China

Abstract

During the weapon airdrop, intricate multi-field coupling interferences arise. This study addresses these complexities by integrating an aeroelastic analysis of the missile body. We have formulated a dynamic, two-way fluid-solid coupling simulation strategy grounded in the Computational Fluid Dynamics/Computational Solid Dynamics with 6 Degrees of Freedom (CFD/CSD-6DOF) methodology. By employing the Arnold Engineering Development Center (AEDC) model as our research focus, we have thoroughly examined the influence of crucial design parameters, including the separation Mach number, altitude, angle of attack, mounting mode, and cavity length depth ratio on the separation. The results indicate that the Mach number significantly impacts the missile's external flow field. During the span and supersonic phases, the missile's shock wave significantly alters the axial and course displacement velocities, with the roll attitude angle undergoing nonlinear variations. The separation altitude determines the local dynamic pressure, revealing that a stable separation attitude can be achieved within a specific altitude range. The high lift generated at the high Angle of attack will prevent the missile from separating from the aircraft. The greater the Angle of attack, the greater the aerodynamic lift and the greater the separation difficulty. Notably, the mounting mode exerts a substantial influence, particularly in Internal-Buried Missile separation scenarios, where complex shear flow interference in the missile compartment heightens the separation risk. The flow field of the Internal-Buried Missile cavity is mainly affected by the length depth ratio. The distribution of pressure in the open cavity flow is more uniform, which is more conducive to the safe separation.

Keywords: Aircraft-missile separation; Aeroelastic effect; Fluid-solid coupling; CFD/CSD-6DOF; Separation parameters

1. Introduction

The safe separation of missiles from the mounting position of military aircraft at high speed is one of the most challenging problems in aircraft design. The safe separation is critical for aircraft safety and missile trajectory precision. As a typical multi-body motion problem, the aircraft-missile separation follows complex dynamic nonlinear flow field interference. On the one hand, the flow field of the aircraft affects the initial separation environment of the missile. On the other hand, the separation is always reestablishing a new unsteady flow field environment, constantly changing the aerodynamic and motion properties of the aircraft and missile. Therefore, various reasons influence the possible domain for missile separation.

The current research methods for aircraft-missile separation mainly include experiments and simulations [1,2,3]. Because of the high risk and cost of the test, multi-body separation simulation based on CFD has become a mainstream research method of aircraft-missile separation [4]. Many researchers have conducted safety analyses of aircraft-missile separation from various perspectives [5]. Panagiotopoulos and Kyparissis [6] analyzed the surface pressure distribution and trajectory

parameters at different angles of attack (α = 0°, 3°, 5°) for external missile separation. They determined the calculation time step based on efficiency and accuracy. Zhu et al. [7] studied the impact of the angle of attack on missile separation. The study found that when the angle of attack is large (α = 10°, 15°, 20°), the distance between the missile and aircraft is small, which poses a threat to the safety and stability of the missiles. Sun et al. [8] used the CFD-6DOF method to conduct a numerical calculation on weapon separation with Mach numbers ranging from 4 to 10. They summarized the influences of flow field properties, Mach number, and angle of attack on the missile separation attitude. Among these, the low Mach number, external mounting missile, and small initial angle of attack had the highest success rate. Shu et al. [9] set up a numerical method for missile separation by considering the aeroelasticity. The results show that Mach number and altitude are two important parameters in the Internal-Buried Missile separation.

Recent studies on aircraft-missile separation have focused on rigid bodies, and few researchers consider the aeroelasticity [10,11,12]. As aerospace science has advanced, aircraft designers have adopted various new composite materials, and the aeroelasticity impact with high-speed separation is becoming increasingly obvious [13]. The fluid-solid coupling effect impact seriously on the separation, especially for large slender missiles. Therefore, based on the CFD/CSD-6DOF, this paper builds a two-way fluid-solid coupling method for aircraft-missile separation considering aeroelasticity. It analyzes the influence of external environmental parameters (Mach number, altitude, angle of attack) and aircraft-missile design parameters (mounting mode, cavity length depth ratio) on separation. This paper is to provide a reference for the safe separation of aircraft and missiles designed by advanced aircraft.

2. CFD/CSD-6DOF two-way coupling method considering the Aeroelasticity

The separation procedure between aircraft and missile has intricate flow field interference (Figure 1) [14,15]. On the one hand, the cylindrical missile shows the characteristic of unsteady separation, the shock wave and separate flow around the aircraft may interfere and fuse at transonic or supersonic. These complex flows moving downstream will interfere with the aircraft's external field characteristics. On the other hand, interference from aircraft, pylon, and missile will also impact the flow field properties of the missile [16].

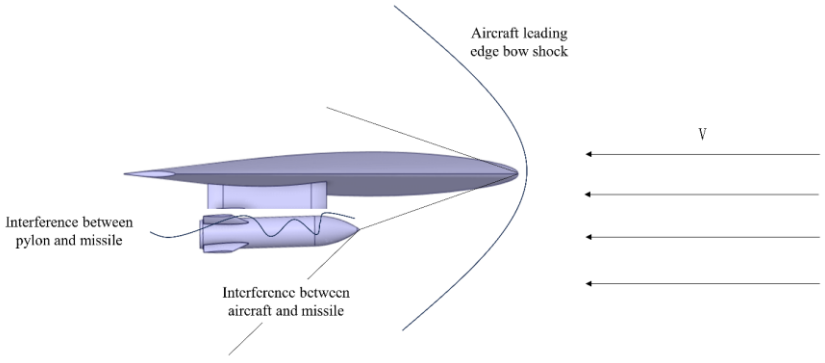

Figure 1 – Aerodynamic interference of aircraft-missile separation

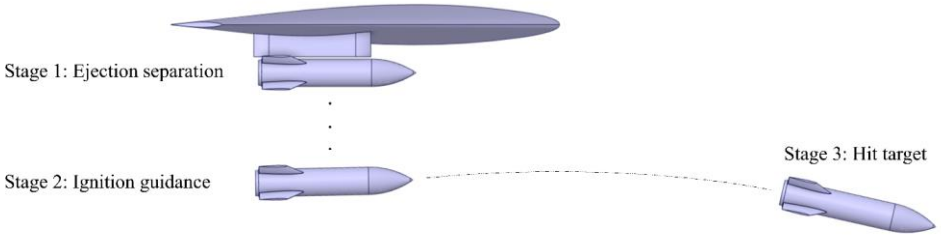

Figure 2 – Aircraft-missile separation process

When the intricate flow field is applied to the slender body missile, especially to the wing, the structural shape of the missile will be changed. On the other hand, the aerodynamic characteristics of deformed structures under this complex flow field will be very different with the accumulation of time. This aerodynamic-structure coupling problem would interfere with the accuracy of missile separation and even threaten the safety of the aircraft. During separation, the missile is removed from the pylon of the aircraft by the ejection force or its gravity, and is released to a certain height following ignition into the guiding task (Figure 2). Therefore, the missile is a key part of the separation, and the aeroelastic effect deserves closer attention. This paper conducts the CFD/CSD-6DOF two-way fluid-solid coupling method considering the solid characteristics of the missile.

The CFD/CSD-6DOF two-way fluid-solid coupling method needs to consider not only the influence of missile aerodynamic force on its structure but also the influence of deformation and the six-degree-of-freedom motion on the flow field. Therefore, the two-way fluid-solid coupling method in this paper is different from the typical method, and its simulation idea follows:

1) In the CFD calculation, it solves the unsteady fluid control equation to gain the aerodynamic force of the missile body. Then the aerodynamic force is transferred to the missile solid grid by using the fluid-solid coupling surface.

2) In the CSD-6DOF calculation, it solves the 6DOF equation of the missile under aerodynamic force to gain the displacement and attitude angles. Then it calculated the response of the solid structure, including the elastic deformation and stress. The final displacement would transfer to the fluid domain by the fluid-solid coupling surface, which equals the centroid displacement plus elastic deformation.

3) The mesh deformation module uses the dynamic mesh method to gain a new flow field mesh under displacement conditions and solves the flow field again.

4) Repeat steps 1-3, and wait for the result to converge or reach the maximum iterations to move on to the next step.

The process of solving the two-way fluid-solid coupling in a single-time step is shown in Figure 3.

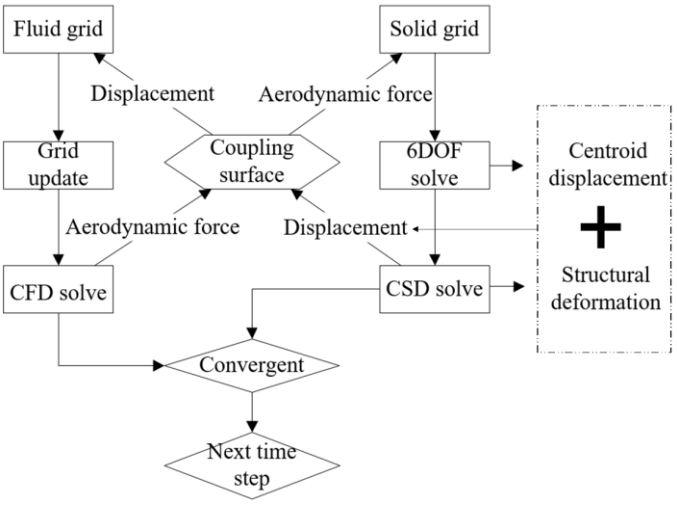

Figure 3 – The process of solving the two-way fluid-solid coupling of CFD/CSD-6DOF in a single-time step

To calculate the aerodynamic force accurately, considering the viscosity of the gas, this paper selected the Reynolds-averaged Navier-Stokes equations (RANS) method and the finite volume method. It uses the second-order Advection Upstream Splitting Method (AUSM) scheme for the advection term and the central difference scheme for the viscosity term.

The fluid causes the solid to distort and move. The solid governing equation follows:

$$M_S\ddot{u} + C_S\dot{u} + K_S u = F \tag{1}$$

Where Ms is the mass matrix, Cs is the damping matrix, Ks is the stiffness matrix, F is the external force borne by the structure, $\ddot{u}$、$\dot{u}$、u are the acceleration, velocity, and displacement. The numerical solution is carried out by using the Newmark implicit time integration method.

At the coupling interface between fluid and solid, the mutual coupling variables such as displacement and stress of fluid and solid are equal or conservative, so the governing equation is

$$\begin{aligned} n \cdot \tau_f &= n \cdot \tau_s \\ r_f &= r_s \end{aligned} \tag{2}$$

Where τ, r are the stress and displacement at the fluid-solid coupling surface, n is the normal unit vector at the coupling surface, the lower corner f represents the fluid, and the lower angle s represents the solid.

The coupling module transfers data between fluid and solid grids at the coupling interface. No matter whether the two grids match exactly or not, the data transfer can be completed well. The profile preserving method transfers non-conservative variables (displacement) (Figure 4). All receiving end nodes match with sending end units one by one, and the data would be transmitted to the receiving end after interpolating at the sending end. The conservative profile-preserving method transfers the conserved variable (force). It adopts multiple methods such as unit partition, pixel concept, bucket algorithm, and new control surface to complete data transfer [17,18]. Accurate transfer of data from global to local is possible at the fluid-solid interface when the fluid grid fully conforms to the solid grid. To keep tight conservation transfer when the mesh at the coupling surface is not similar, the conservative profile-preserving method ignores the data transfer by setting special boundaries and 0 values in the non-conservative region [19] (Figure 5).

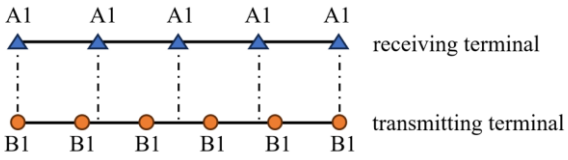

Figure 4 – Profile-preserving for data transmission

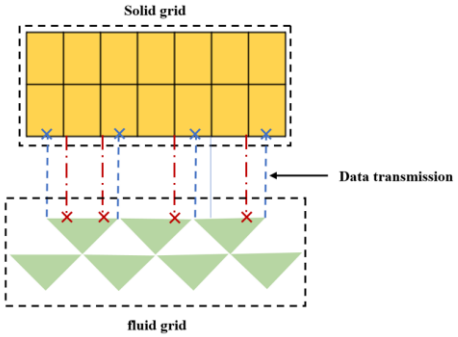

Figure 5 – Conservative profile-preserving for data transmission

3. Simulation Verification of Aircraft-missile Separation Considering the Aeroelasticity

3.1 Model and grid

AEDC is a classic example of aircraft-missile separation [20]. The model is shown in Figure 6. The origin of the coordinate is the warhead and the missile mass is 907kg. To separate the missile from the aircraft quickly, the ejection forces of 10.7KN and 42.7KN are applied at x=1.2375m and x=1.7465m for 0.054s. The working condition of the test is an altitude of 11.6km, the Mach number is 1.2 and the angle of attack is 0 degrees.

This section simulates the AEDC standard model separation based on the CFD/CSD-6DOF coupling method in section 2 first. It is necessary to create a fluid and solid grid. The slenderness ratio of the AEDC missile is 5.9. Under aerodynamic force, the missile's wing has the most elastic deformation, whereas the body has little. Besides, the small deformation has little influence on the missile separation (changes in centroid displacement and attitude angle). Therefore, this paper adopts the

solid model to build the solid grid and sets a concentrated mass point at the head to simulate the moment of inertia and center of mass position in the test. The material properties of the missile are shown in Table 1 below.

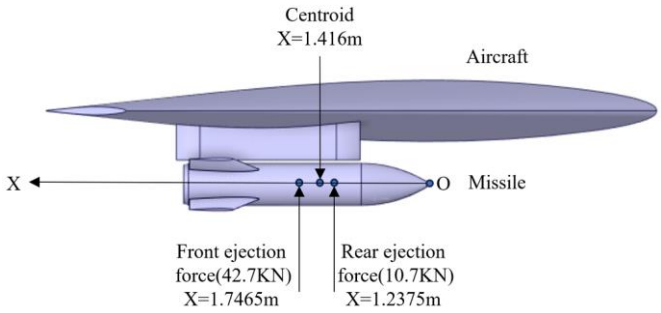

Figure 6 – AEDC geometric model

Table 1 AEDC Missile structural material properties

Missile mass(kg)	907
Position of center of gravity (m)	(1.416,0,0)
Moment of inertia (kg·m2)	IXX=27.12 IYY=488.1 IZZ=488.1
Reference area (m2)	0.2028
Reference length (m)	0.508

Figure 7 is the missile solid grid, the grid type is tetrahedron and the grid size is 110000. At the same time, the coupling interface is set up, and the value at the coupling interface is interpolated using the profile-preserving method. The data transfer is accurate when the fluid-solid grid scale is 0.03m.
Figure 8 is the fluid grid at the initial state, and the grid size is 1.84 million. In this paper, time advance is double time steps, the physical time step is 0.0005s and the iteration step is 20.
The CFD module uses smoothing and remeshing methods to update the grid in real time to adapt to continuously moving objects. And it refines the mesh below the aircraft to improve calculating accuracy.

(a) **(b)**

Figure 7 – Solid model and grid of missile: (a)model; (b)grid

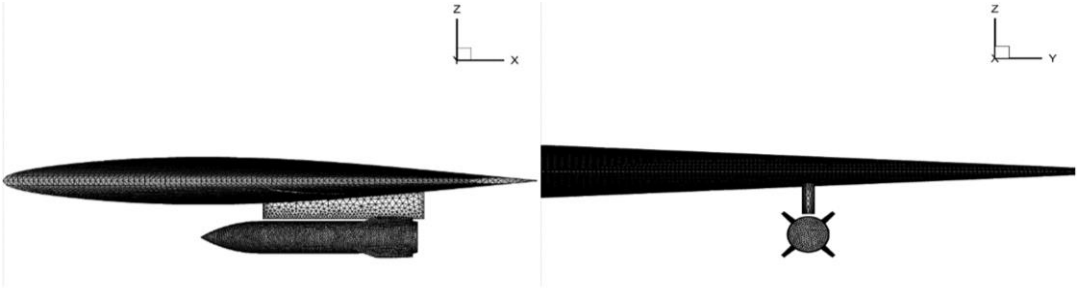

Figure 8 – CFD computing grid

3.2 Verification and comparison of separation considering aeroelasticity

The aircraft-missile separation simulation considering the aeroelasticity is carried out based on CFD/CSD-6DOF. Figure 9 and Figure 10 show the missile's centroid displacement, velocity, and attitude changes. To prove the influence of aeroelasticity, this study compares simulation results with test data. From the results, the aeroelastic effect has a great influence on the aircraft-missile separation. The displacement and velocity errors in the y-direction are slightly large. On the one hand, the displacement and velocity values in the y direction are small, even a small disturbance might cause large errors. On the other hand, the roll angle and yaw angle are smaller than the test values, and the side force of the missile in this state is smaller, resulting in smaller displacement and velocity in the y direction. Besides, the moment of inertia of the missile around the x-axis is eighteen times smaller than that of the other two axes, and roll angle changes are more sensitive, making accurate simulation difficult. At 0.8s, the pitch angle error is about 4.3 and the yaw angle error is about 1.2 °. The displacement and velocity calculated by CFD/CSD-6DOF are close to the test values, whereas the attitude angle error is slightly greater.

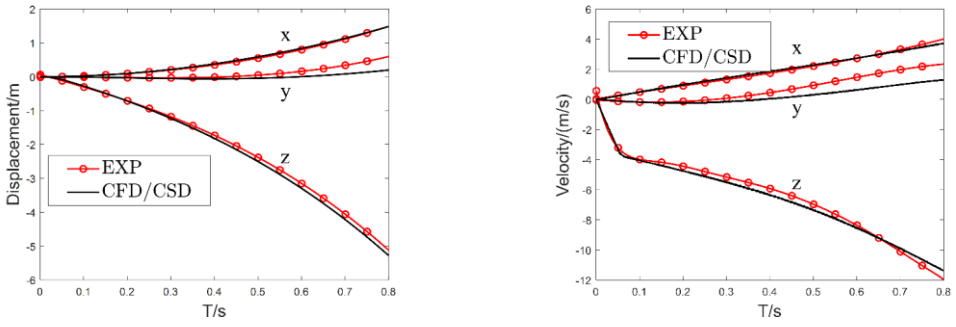

Figure 9 – Missile centroid displacement and velocity: (a) displacement; (b) velocity

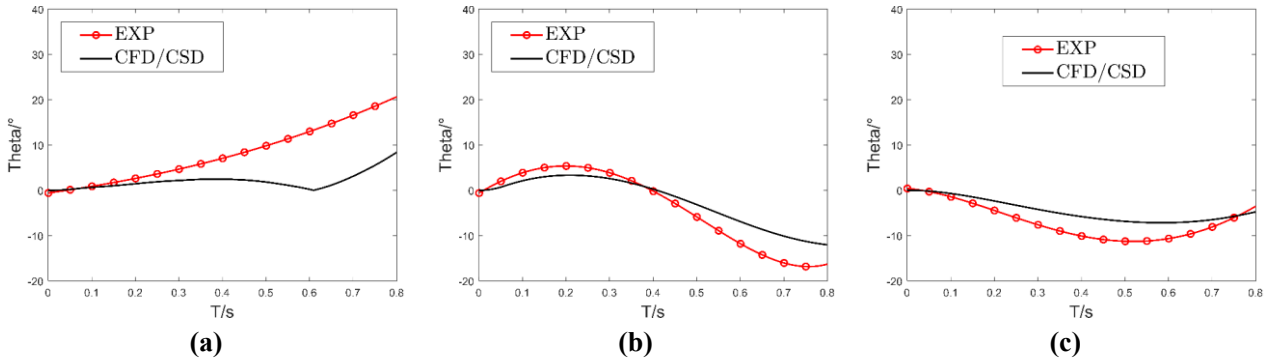

Figure 10 – Missile attitude angle: (a)roll angle; (b) pitch angle; (c)yaw angle

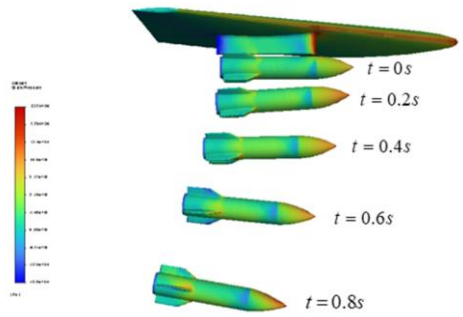

Figure 11 – Missile drop trajectory of the CFD/CSD-6DOF

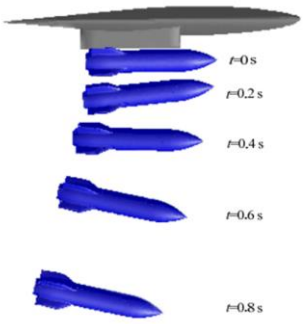

Figure 12 – Missile drop trajectory of the test

Figure 11 and Figure 12 are the missile drop trajectories based on the CFD/CSD-6DOF and test results. Comparing the missile's position and attitude at different times, that reveals aeroelasticity has an obvious effect on the falling trajectory and roll angle.

4. Analysis of influence parameters in the process of aircraft-missile separation

Various parameters affect the aircraft-missile separation, which is mainly divided into external environmental parameters such as Mach number, flight altitude, and angle of attack, and aircraft-missile design parameters, such as mounting mode, and cavity length depth ratio. The impact of each parameter is different, specifically:

Mach number: Mach number determines the velocity environment of aircraft-missile separation, which makes the aerodynamic environment of the missile itself more complex. For example, in the transonic and supersonic phases, the strong shock wave induced by the missile body leads to a change in the focus of the missile body and leads to a drastic change in attitude.

Separation altitude: Altitude affects the aerodynamic force of the missile through density and air pressure, while coupling Mach number interferes with the flow field environment, altering the missile's attitude response after separation.

Angle of attack: The high lift generated at the high Angle of attack will prevent the missile from separating from the aircraft. The greater the Angle of attack, the greater the aerodynamic lift and the greater the separation difficulty.

Mounting mode: Different mounting methods have distinct initial flow field properties, so the beginning environment and the stress of the separation differ significantly. The external-mounted type has less interference on aircraft-missile separation while the internal-buried type has the most. Because the internal-buried one needs a complicated push-separation procedure. Especially when the missile passes through the shear layer of the buried cabin, the strong nonlinear flow field will seriously affect the force of the missile and change the separation characteristics.

Cavity length depth ratio: The length depth ratio of Internal-Buried Missile mainly affects the cavity flow field characteristics. Different flow types have different pressure distribution rules for the cavity, which influence the aircraft-missile separation.

This section will investigate the impact of missile Mach number, altitude, angle of attack, mounting mode, and length depth ratio on the missile separation using the CFD/CSD-6DOF two-way fluid-solid coupling method. To explore the effects of different parameters efficiently on the flow field characteristics and missile trajectory attitude in the aircraft-missile separation, the test design is illustrated in Table 2. Except for the 4.4 and 4.5 sections, which differ from the AEDC standard model, the other models are shown in Figure 6.

Table 2 Design of experiment table

Parameters	Design 1	Design 2	Design 3	Design 4
Mach number	0.3	0.6	0.9	1.2
Altitude /km	6	9	11.6	-
Angle of attack/°	0	4	8	12
Mounting mode	External-mounted	Semi-buried	Internal-buried	-
Length depth ratio	5	10	15	-

4.1 Separation Mach number

This section simulates aircraft-missile separation at Mach numbers of 0.3Ma, 0.6Ma, 0.9Ma, and 1.2Ma based on the CFD/CSD-6DOF two-way fluid-solid coupling method. The results are shown in Figure 13. During the missile separation, the x-direction displacement of the mass center increases obviously with the growth of the Mach number. Especially at Mach numbers of 0.9Ma and 1.2Ma, the missile warhead would cause higher-intensity shock waves. It would strengthen the shock wave drag which is reflected in the increase of x-direction displacement. For the y-direction displacement of the center mass, it is smaller at a low Mach number and moves slightly in the range of (- 0.1) m. The y-direction displacement is uncertain at a high Mach number. On the one hand, the displacement range is larger than that of a low Mach number. On the other hand, the displacement direction will be reversed at 0.6s of 0.9Ma and 0.4s of 1.2Ma. Figure 13(b) shows that when the Mach number increases, the x-direction velocity increases significantly and varies linearly with time. The y-direction velocity is small at a low Mach number, decreases at first, and then increases at 0.2 ~ 0.3s when it is higher than 0.9Ma. This is because the missile faces an asymmetric aerodynamic force on the longitudinal symmetry surface during the launch, and the higher flight pressure makes the missile gain a larger initial side force. The side force acting on the wing and body changes easily the side displacement and velocity of the missile. In addition, at 0.2s and 0.3s, the side force of the missile under the launching velocity of 0.9Ma and 1.2Ma changes from negative to positive, which changes the missile acceleration direction.

As shown in Figure 13(c) is the change of attitude angle. At low Mach numbers, the roll angle of the missile varies linearly, whereas at high Mach numbers, the shift takes the form of a "wave," that is, "increase-decrease-increase". For the pitch angle, the missile is always pitching up in the whole procedure at a low Mach number, and the pitch angle is positive. At a high Mach number, the missile changes from pitch up to down and pitch angle from positive to negative at 0.4s.

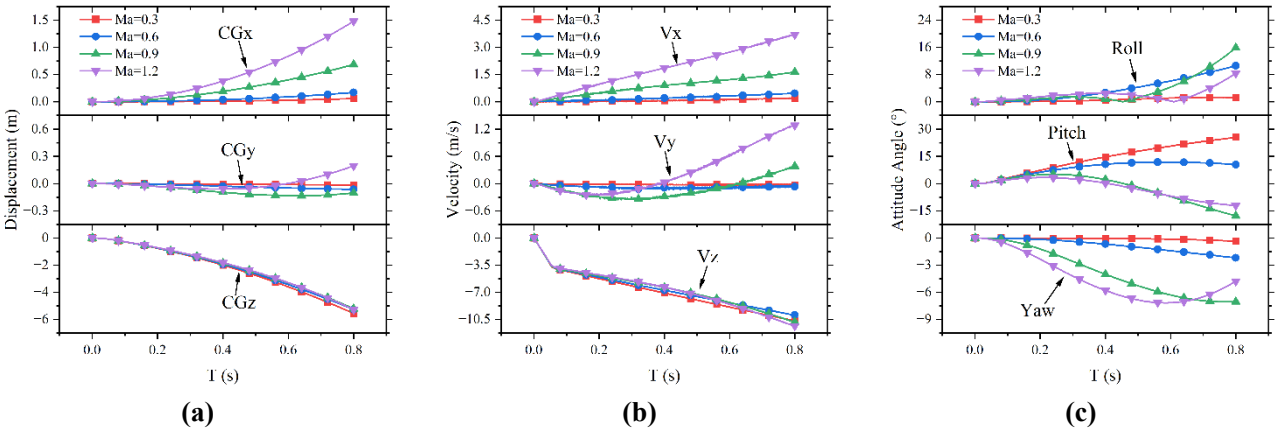

Figure 13 – Simulation results of aircraft-missile separation at different Mach numbers: (a) Displacement; (b) Velocity; (c) Attitude angle

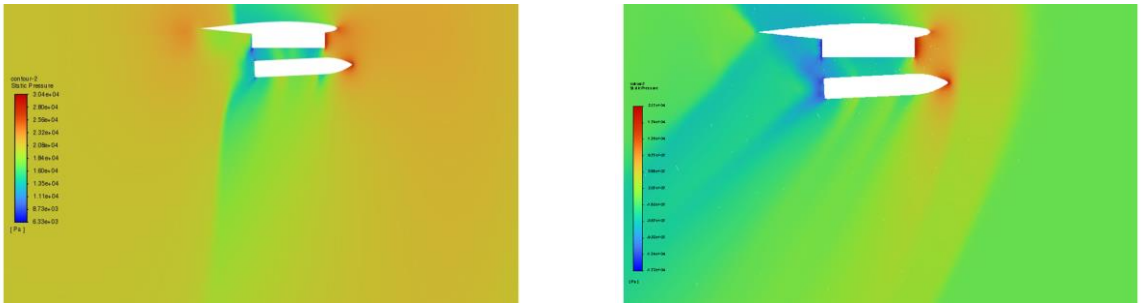

(a) (b)

Figure 14 – Pressure cloud map at different Mach numbers: (a) "0.9Ma release" at 0.1s ; (b) "1.2Ma release" at 0.1s

In addition, as the Mach number increases, the change in yaw angle gets more complex. When the aircraft's delivery speed reaches 1.2Ma, an obvious bow shock wave will form on the aircraft's leading edge. The missile also produces oblique shock waves of different intensities at the wing and body of the missile. The intensity of the shock wave produced by 0.9Ma is weaker than that of 1.2Ma, but the airflow near the missile wing will still compress, resulting in the shock wave. The flow field is more complex when the shock wave exists, and it is more difficult to control and navigate accurately.
The Mach number is an important parameter that affects the accuracy and safety of missile separation. At a low Mach number, the missile is less disturbed by aerodynamic loads and it may change trajectory and attitude by adjusting the rudder. While at a high Mach number, we must consider the influence of shock waves on the launch. Complex physical interference phenomena such as shock wave, shock wave/expansion wave, shock wave / shear layer, and shock wave/boundary layer may occur [21]. The generation and propagation of shock waves will lead to a change in aerodynamic force and uneven pressure distribution. This shock wave interference will significantly impact the missile's stability and flight performance. On the other hand, the missile dropped by the high-speed aircraft can reach the target faster and produce more striking force. However, the oblique shock wave is easily produced when the high-speed missile passes through the bow shock wave at the aircraft's leading edge, and the flow field is relatively more complex.

4.2 Separation altitude

Figure 15 reflects the displacement, velocity, and attitude changes of missile separation at the altitudes of 6km, 9km, and 11.6km. In the missile separation, the x-direction displacement decreases dramatically with the increase of the altitude. This is because the lower the altitude, the higher the flying pressure, and the greater the x-direction drag of the missile. It leads to an increase in the x-direction displacement of the missile mass center. For the y-direction displacement of the center of mass, three missiles move slightly in the range of -0.2m to 0m during the early period. As the release altitude grows, the three missiles start moving in the positive direction y at 0.28s, 0.33s, and 0.39s, and the missile’s falling distance reduces. The x-direction velocity increases remarkably and linearly with the increase of the altitude of the missile, and the y-direction velocity changes from negative to positive at 0.28s, 0.33s, and 0.39s. In addition, different from "9km release" and "11.6km release", the y-direction velocity of the "6km release" missile will decrease after reaching the maximum value at 0.65s.

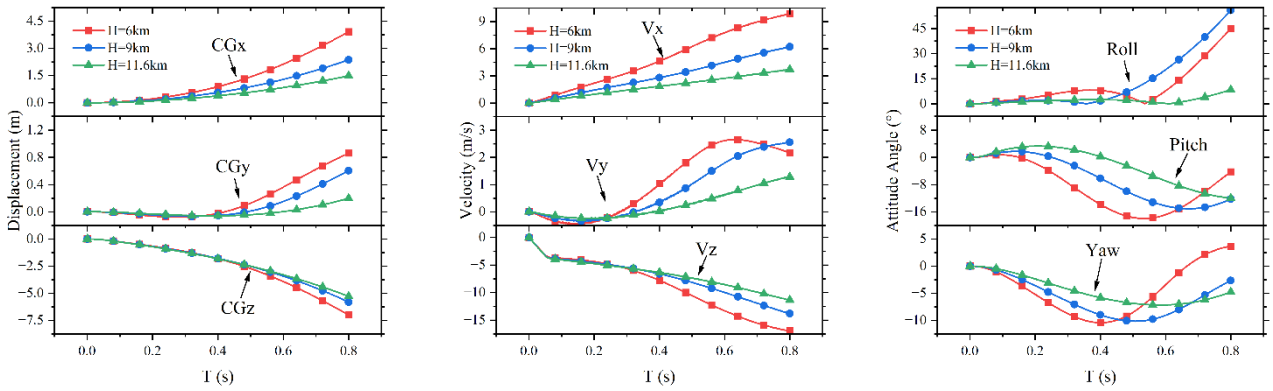

Figure 15 – Simulation results of aircraft-missile separation at different altitudes: (a) Displacement; (b) Velocity; (c) Attitude angle

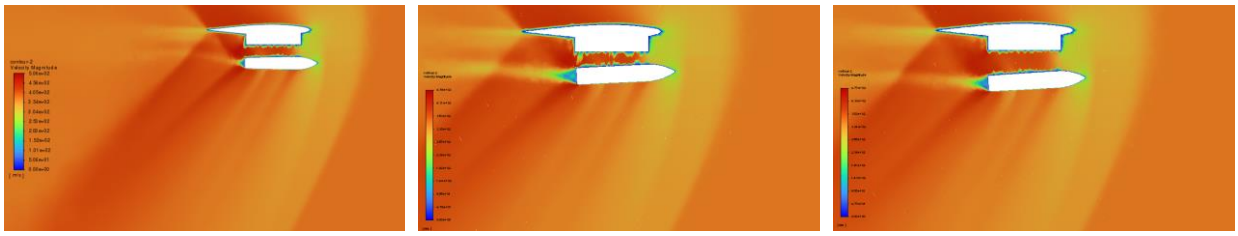

Figure 16 – Missile velocity cloud map at different separation altitudes: (a) "6km release" at 0.15s; (b) "9km release" at 0.25s; (c) "11.6km release" at 0.15s

The roll angles of the three missiles vary sensitively and violently because the moment of inertia of the missile around the x-axis is eighteen times smaller than that of the other two axes. At the final time t=0.8s, the roll angle of "6km release" is 45 °, "9km release" is 56 °, and "11.6km release" is 8.4 °. In the separation, the missile briefly raised its head and then bowed its head, and the critical points were 0.15s of "6km release", 0.25s of "9km release" and 0.41s of "11.6km release". After reaching the pitch angle valley (about 15 degrees), the bow attitude decreases under the pitch-up moment, and the missile has longitudinal static stability. For the yaw angle range, the lateral force of the missile with low release altitude is larger, and the yaw angle changes more rapidly.

Table 3 Dynamic pressure at different altitudes

Separation altitude /km	6	9	11.6
Dynamic pressure /Pa	47660	31044	20931

The pitch angles of missiles launched at different altitudes can change from positive to negative after separation, which ensures a safe separation from the aircraft. Figure 16 is the missile velocity cloud map of three kinds of release altitudes, and the velocity distribution is similar. As shown in Table 3, the lower the release altitude, the higher the dynamic pressure and the aerodynamic force generated by the missile [22]. Thus, it is difficult to control the missile accurately at a low release altitude for greater disturbance.

4.3 Angle of attack

This section simulates aircraft-missile separation at four different angles of attack, alpha = 0,4,8,12. Figure 17 shows the change in the missile's displacement, velocity, and attitude angle during the separation. With the increase of the angle of attack, the displacement and velocity of the missile in

the x and z direction are smaller, and the displacement and velocity in the y direction are larger. In addition, for the attitude angle, the roll angle and yaw angle of the missile change more greatly under the large attack angle. In particular, the peak pitch angle of "alpha=0°" is 3.3° and that of "alpha=12°" is 6.5°, which increases the potential danger of aircraft-missile separation.

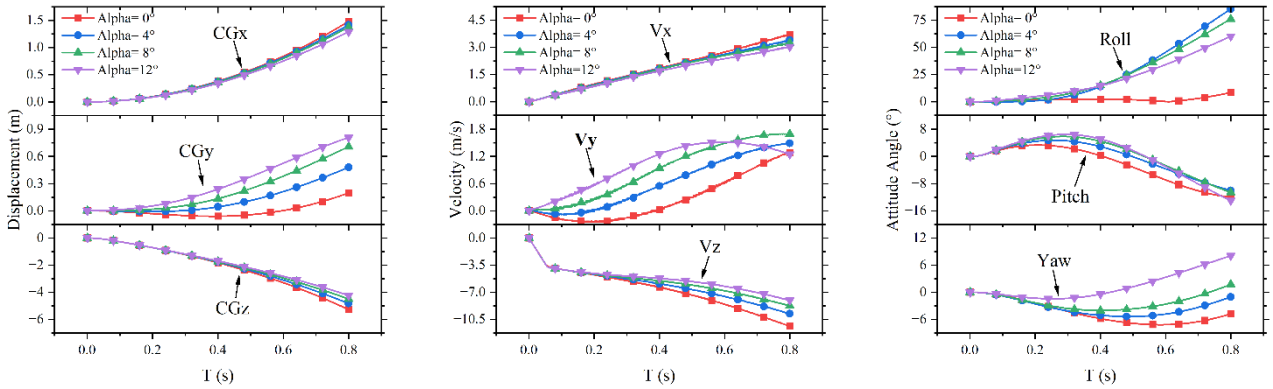

Figure 17 – Simulation results of aircraft-missile separation at different angles of attack: (a) Displacement; (b) Velocity; (c) Attitude angle

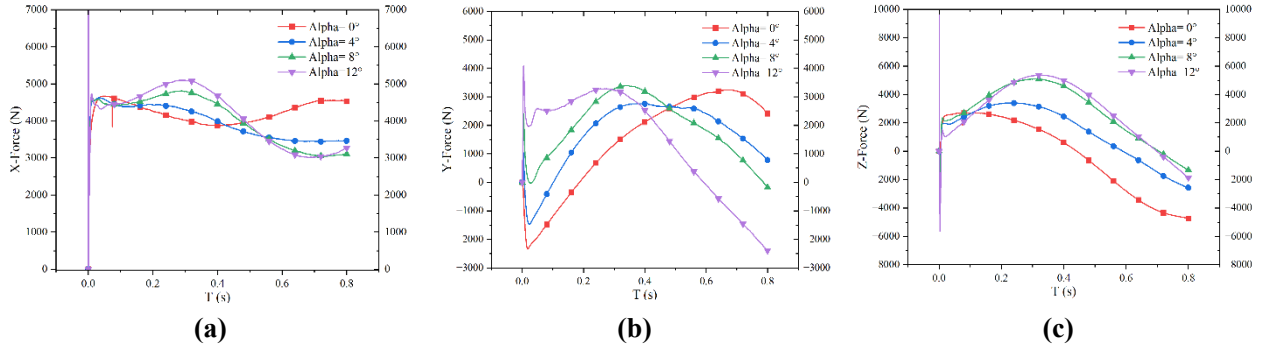

Figure 18 – Three-direction force curve of the missile at different angles of attack:(a)X-Force; (b)Y-Force; (c)Z-Force;

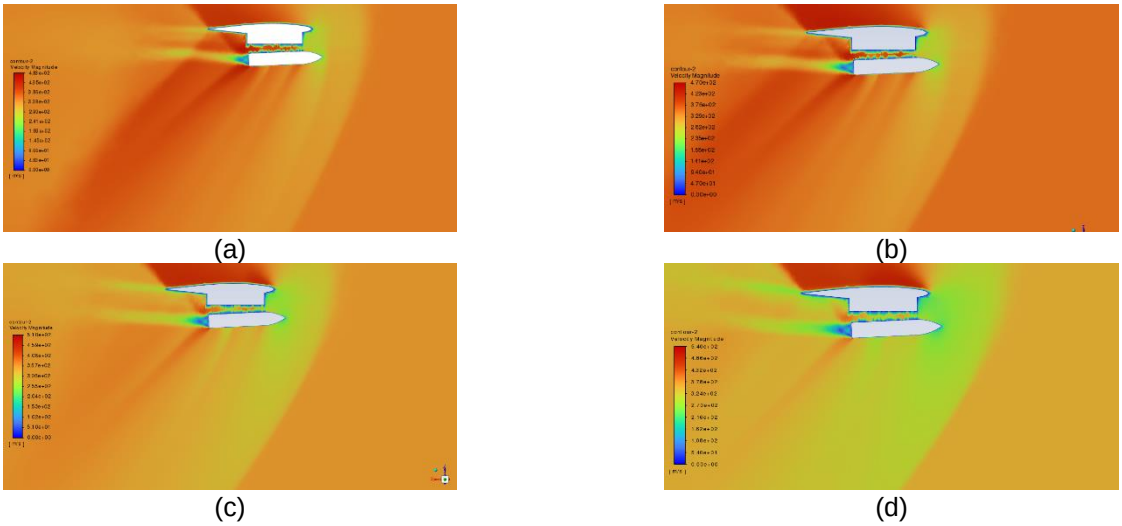

Figure 19 – Pressure cloud map at T=0.1s at different angles of attack:(a)Alpha=0°; (b) Alpha=4°; (c) Alpha=8°; (d) Alpha=12°

Figure 18 and Figure 19 show the three-direction force curve of the missile and the pressure cloud map at t=0.1s. The pressure is higher at the missile's bottom at the high angle of attack. After the downward ejection force disappears, the missile cannot resist the aerodynamic lift of the incoming flow by its gravity. This high lift will prevent the missile from separating from the aircraft. The larger the angle of attack, the stronger the aerodynamic lift and the more difficult the separation. In addition, the missile's large pitch-up attitude at the high angle of attack would pose a serious threat to the safety of the separation.

4.4 Mounting mode

According to the mounting form of aircraft weapons, missiles are mainly divided into three types: Internal-Buried Missile (IBM), Semi-Buried Missile (SBM), and External-Mounted Missile (EMM). The IBM is completely loaded into the aircraft, which takes up a large internal space. And the aircraft's drag would not reduce step-by-step after loading the missile [23,24,25]. The SBM buries part of the weapon into the missile bay, while the other part is exposed. This form of loading contributes to reducing drag, but slotting increases structural weight. It lacks interchangeability because it can only be equipped with weapons of a certain shape. The EMM hangers at the wing and the lower surface of the aircraft, which is widely used in vintage fighters [26].

As shown in Figure 20, the geometric models of IBM, SBM, and EMM are all the same type of aircraft in this paper. The IBM is fully loaded in the missile bay, the SBM is half-loaded, and the EMM hangers at the lower part of the missile bay. Based on the basic working conditions, this section simulates the aircraft-missile separation in the three cases and analyzes the law of mounting mode.

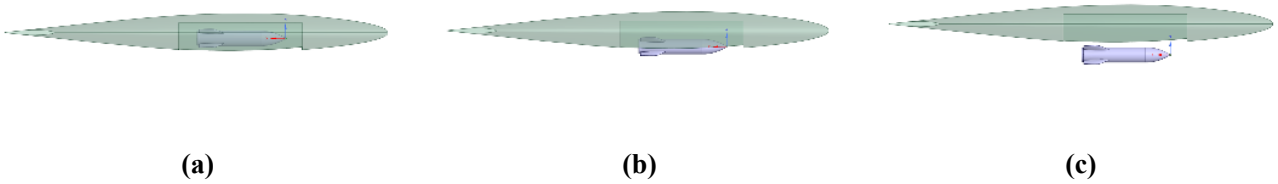

(a) (b) (c)

Figure 20 – Geometric models of different mounting modes: (a)IBM; (b)SBM; (c)EMM

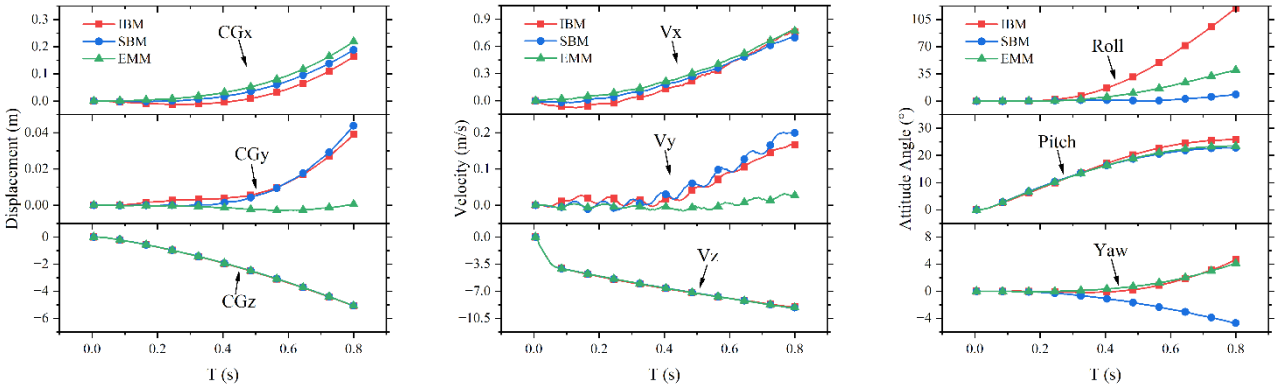

(a) (b) (c)

Figure 21 – Simulation results of aircraft-missile separation of different mounting modes: (a) Displacement; (b) Velocity; (c) Attitude angle

Figure 21 shows the displacement of the missile. Different from the IBM and SBM, the EMM has a negative x-direction displacement for the first 0.43s in the missile separation. For the y-direction displacement of the center of mass, the displacements of the three modes are all very small, the maximum is only 0.045m, and the lateral displacement of the EMM is almost 0.

In addition, Figure 21(c) shows the change in missile attitude angle. The roll angle is 119.8° at 0.8s for IBM, 8.5° at 0.8s for SBM, and 40.1° for EMM. The missiles of the three mounting modes are all pitching up all the time, and the trend is no longer increased after 0.8s. Additionally, the influence of the flow field of the IBM is greater, the time is longer, and the peak pitch angle is larger. For the yaw angle, the yaw angle of the IBM and EMM is positive, and the SBM is negative.

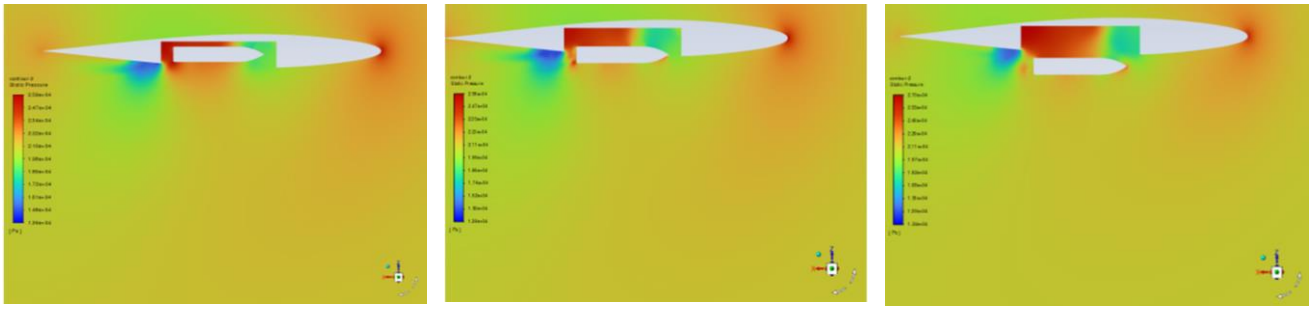

(a) **(b)** **(c)**

Figure 22 – Initial flow field of different mounting modes: (a)IBM; (b)SBM; (c)EMM

Figure 22 is the pressure cloud map of the three mounting modes at 0s. Due to the large chamber, when the flow goes through the chamber's leading edge, it will bend in the inner wall, and an upwash flow forms in the front area [27]. Then it flows backward close to the inner wall and bends outward at the rear edge of the chamber, forming a downwash flow in the tail area. Especially when the missile passes through the shearing layer of the missile cabin, the upwash flow forms in the front area of the bay while the downwash flow forms in the back. The whole impact will form a pitch-up moment, thus showing a larger pitch-up attitude. The missiles with three kinds of mounting modes will affect the separation in varying degrees, and the order of influence is Internal-Buried Missile > Semi-Buried Missile > External-Mounted Missile.

4.5 Cavity length depth ratio

The separation characteristics of the Internal-Buried Missile are closely related to the flow field of the cavity, which is mainly affected by the length depth ratio (L/D). The flow of the cavity can be divided into open cavity flow (L/D<10), transition flow (10≤L/D≤13), and closed cavity flow (L/D>13). In Figure 23, the simulation model selects three typical cavities, L/D=5,10,15.

(a) **(b)** **(c)**

Figure 23 – Simulation models: (a) L/D=5, open cavity flow; (b) L/D=10, transition flow; (c) L/D=15, closed cavity flow

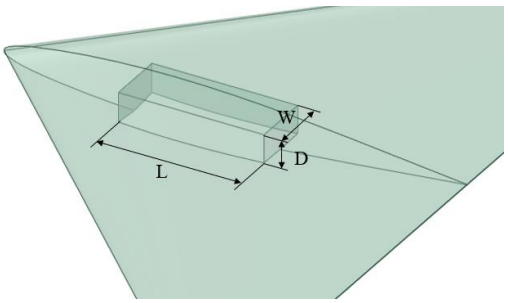

Figure 24 – The parameter of the Internal-Buried cavity diagram

Table 4 The parameter of the simulation model

No.	Width/mm	Length/mm	Depth/mm	L/D	Flow type
1			1000	5	open cavity flow
2	2000	5000	500	10	transition flow
3			333	15	closed cavity flow

The displacement value of the "L/D=15" missile in the x and y directions is smaller than that of the other two missiles. But in the falling z direction, it falls faster, and the z velocity is greater. Regarding attitude angle, the three attitude angles of the "L/D=5" missile change less, and the flight attitude is more stable. Especially the pitch angle, the "L/D=5" missile has been in a small pitch-down attitude (-6°<pitch angle<0°), the "L/D=10" missile is 0°~24.9° and the "L/D=15" missile is 0°~40.0°.

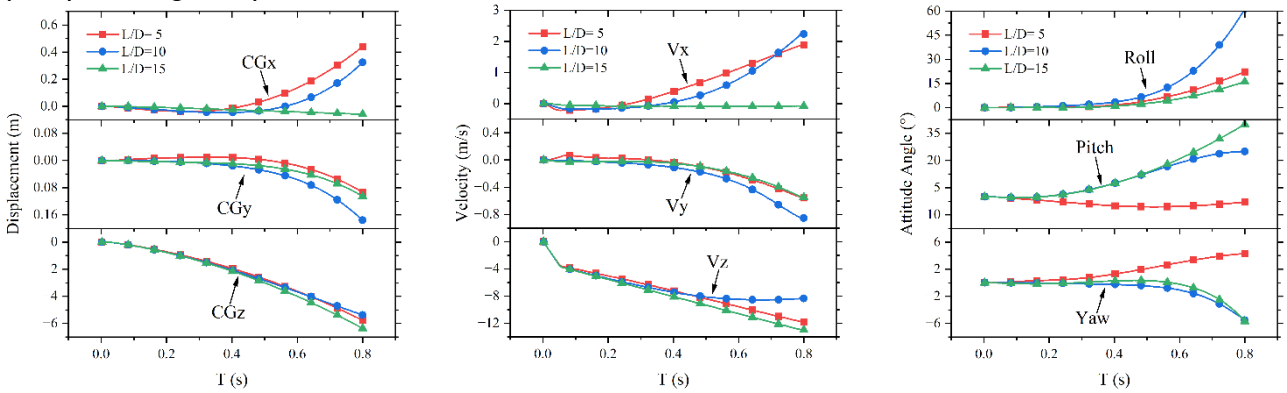

Fig. 25 – Simulation results of aircraft-missile separation of different length depth ratios: (a) Displacement; (b) Velocity; (c) Attitude angle

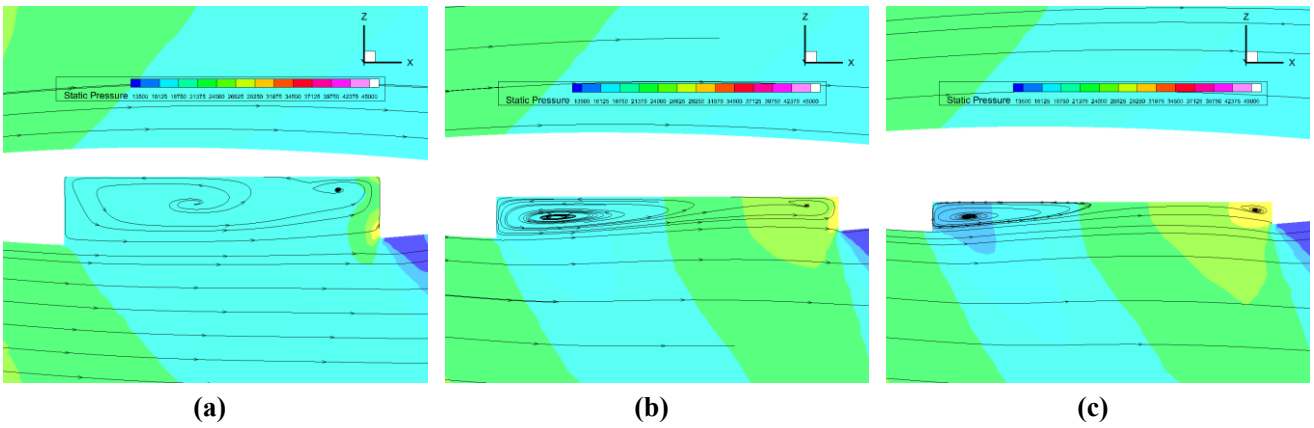

Figure 26 – Different cavity flow type: (a) L/D=5, open cavity flow; (b) L/D=10, transition flow; (c) L/D=15, closed cavity flow

For open cavity flow (Figure 26(a)), the shear layer directly crosses the cavity as the air flows through it. The expansion low-pressure area in the front cavity wall and the high-pressure area in the back cavity wall will be connected, forming a vortex and having a vortex center. The low pressure at the front and the high pressure at the back of the cavity are balanced, and the pressure at the bottom of the cavity is evenly distributed.

For closed cavity flow (Figure 26(c)), when the air flows through the cavity, the air expansion pressure at the front wall is reduced, and a vortex is generated to form the upwash area of the airflow. The

middle part of the shear layer is deflected upward by the influence of the upwash area of the airflow, which will impact the cavity bottom and increase the pressure. Then the air would hit the cavity back wall, and the pressure would rise again. In the cavity back wall formed a downwash due to the pressure gradient.
In short, the distribution of pressure in the open cavity flow is more uniform, and the flow characteristics of the cavity are more stable, which is more conducive to the safe separation and launch of the Internal-Buried Missile.

5. Conclusion

This paper sets up a two-way coupling simulation method of aircraft-missile separation considering aeroelasticity based on CFD/CSD-6DOF, analyzes the AEDC standard model separation, and studies the effects of Mach number, altitude, mounting mode, additional ejection force and missile tail thrust on the separation. The main conclusions are as follows:
(1) With the increase of Mach number, the aircraft's leading edge would form an obvious bow shock wave, and the missile may also produce different intensity oblique shock waves at the wing and body. When the Mach number is higher (above transonic), the missile changes its axial and heading displacement violently because of the asymmetric aerodynamic forces. For attitude angle, the variation trend of roll angle and yaw angle at high Mach number is complex, especially the roll angle shows the change of "increase-decrease-increase".
(2) Missiles launched from high altitudes provide superior control and navigation. As the separation altitude increases, the flight pressure of the missile separation decreases, and the disturbance will be smaller. The displacement and velocity change slightly of the missile at higher altitudes, and the missile is difficult to yaw. However, the attitude shift is steady, and the change in pitch angular velocity is minor.
(3) The high lift generated at the high Angle of attack will prevent the missile from separating from the aircraft. The greater the Angle of attack, the greater the aerodynamic lift and the greater the separation difficulty. In addition, the missile’s large pitch-up attitude at the high angle of attack would pose a serious threat to the safety of the separation.
(4) Due to the missile bay, the upwash flow forms in the front area of the bay while the downwash flow forms in the back. The missiles with three kinds of mounting modes will affect the separation in varying degrees, and the order of influence is Internal-Buried Missile > Semi-Buried Missile > External-Mounted Missile.
(5) The separation characteristics of the Internal-Buried Missile are closely related to the flow field of the cavity, which is mainly affected by the length depth ratio (L/D).the distribution of pressure in the open cavity flow is more uniform, and the flow characteristics of the cavity are more stable, which is more conducive to the safe separation and launch of the Internal-Buried Missile.

6. Acknowledgement

The authors would like to acknowledge the support of National Natural Science Foundation of China (Grant No. 12202363) and the support of Key Laboratory Fund (Grant No.D5150240005).

7. Copyright Issues

Reference

[1] Anandhanarayanan K, Raj A, Shah V, et al.,2018. Separation Dynamics of Air-to-Air Missile and Validation with Flight Data. Defence Science Journal, 68(1).

[2] Hetreed C, Carroll M, Collard J, et al., 2018. F-35 Weapons Separation Test and Verification. Aviation Technology, Integration, and Operations Conference, p. 3680.

[3] Jiang JJ, Chen LZ, 2024. Dynamic wing tunnel drop testing on internal. Journal of Ordnance Equipment Engineering, 45(1):173-179.

[4] Song W, Ai BC, 2022. Experimental investigation on aircraft-store compatibility and flow control for internal weapons separation. Acta Aerodynamica Sinica, 40(03):203-211.

[5] Wang HZ, Li X, Wang XP, et al., 2017. Safety Assessment for Store Separation. Aerospace Shanghai, 34(05):124-129.

[6] Panagiotopoulos EE, and Kyparissis SD, 2010. CFD transonic store separation trajectory predictions with comparison to wind tunnel investigations. International Journal of Engineering, 3(6), p.538-553.

[7] Zhu SQ, Li HY, Chen ZH, et al., 2018. Inflences of angles of attack during the separation of an air-to-air missile from the aircraft. Engineering Mechanics, 35(09)248-256.

[8] Sun JM, Zuo G, Xu YZ, et al., 2023. Numerical simulation of weapon delivery schemes for hypersonic vehicles in near space. Acta Aeronautica et Astronautica Sinica, 44 (13): 27-42.

[9] Shu LT, Rong JL, Ke X, et al., 2023. Investigation of Aeroelasticity Effect on Missile Separation from the Internal Bay. International Journal of Aerospace Engineering, 2023.

[10] Osman AA, Aly AM, Khalil EE, et al., 2016 Numerical analysis of an external store separation from an airplane. AIAA modeling and simulation technologies conference, p. 2143.

[11] Kim E, Kwon JH, Park SH, et al., 2010. Prediction of ballistic separation effect by direct calculation of incremental coefficients. Journal of aircraft, 47(2): 630-637.

[12] Wang G, Chen X, Xing Y, et al., 2017. Multi-body separation simulation with an improved general mesh deformation method. Aerospace Science and Technology, 71: 763-771.

[13] Ye ZY, Zhang WW, Shi AM, et al., 2010. Fundamentals of fluid-structure coupling and its application, 2nd Edition. Harbin Institute of Technology Press, Harbin, China, p.165-234.

[14] Sun Y, Liu Q, Cattafesta III et al., 2019. Effects of sidewalls and leading-edge blowing on flows over long rectangular cavities. AIAA journal, 57(1): 106-119.

[15] Robertson G, Kumar R, 2020. Effects of a generic store on cavity resonance at supersonic speeds. AIAA Journal, 58(10): 4426-4437.

[16] Yang L, Ye ZY, Wu J, et al., 2016. Influence of elastic to dynamic responses of store. Physics of Gases, 1(4): 1-11.

[17] Rizvi A, Smith CW, Rajasekaran R, et al., 2016. Dynamics of dry friction damping in gas turbines: literature survey. Journal of Vibration and Control, 22(1): 296—305.

[18] Marques F, Flores P, Claro JCP, et al., 2016. A survey and comparison of several friction force models for dynamic analysis of multibody mechanical systems. Nonlinear Dynamics, 86(3): 1—37.

[19] Cui P C, Tang J, Li B, et al., 2018. A conservative interpolation method for overset mesh via supermesh. Acta Aeronautica et Astronautica Sinica, 39(3): 121569.

[20] Zhu SQ, Li HY, Chen ZH, et al., 2017. Numerical investigations on missile separation of an aircraft based on CFD/CSD two-way coupling method. Engineering Mechanics, 34(10): 217-228,248.

[21] Chen B, Luo L, Jiang AL, et al., 2023. Numerical simulation of separation characteristics for internal weapon at high Mach number. Journal of Beijing University of Aeronautics and Astronautics,1-18.

[22] Dong JG, Chen KZ, Feng X, et al., 2021. Experimental investigations on the separation interference characteristics of supersonic internal weapon releasing from the aircraft. Journal of Experiments in Fluid Mechanics, 35(3): 46-51.

[23] Jing SY, 2014. Research on the Flow Field of Weapon Bay and the Trajectory of Missile Separating. PhD Zhang, Nanjing University of Aeronautics and Astronautics, Nanjing,China.

[24] Saddington AJ, Thangamani V, Knowles K, et al., 2016. Comparison of passive flow control methods for a cavity in transonic flow. Journal of Aircraft, 53(5): 1439-1447.

[25] Khanal B, Knowles K, Saddington A, et al., 2009. Computational study of cavity flowfield at transonic speeds. 47th AIAA Aerospace Sciences Meeting including The New Horizons Forum and Aerospace Exposition, p. 701.

[26] Fan JJ, Zhang HR, Guan F, et al., 2018. Studies of aerodynamic interference characteristics for external store separation. Journal of National University of Defense Technology, 40(02): 13-21.

[27] Li H, Yang YY, Zhang J, et al., 2022. Application of DES method in internal weapon separation simulation. Acta Aerodynamica Sinica, 40(3): 190-202.